Basins of attraction for renormalization-group trajectories arising in a spin-1 Ising model with competing biquadratic interactions

Daniel P. Snowman*
Department of Physical Sciences, Rhode Island College, Providence, Rhode Island 02908, USA
(Received 19 March 2007; revised manuscript received 21 March 2008; published 15 April 2008)

The current investigation probes frustration that arises in a Blume-Emery-Griffiths system due to competing biquadratic ($\pm K$) interactions while uniform bilinear and crystal-field interactions are maintained. This competition directly affects the clustering and density of nonmagnetic impurities. All calculations have been conducted using a hierarchical lattice in conjunction with renormalization-group methods. Phase diagrams have been calculated for a series of planes of constant biquadratic coupling while varying the temperature and concentration of annealed vacancies in the system. Each phase diagram reveals three qualitatively unique basins of attraction, each sharing renormalization-group trajectories that flow to common sinks.

DOI: 10.1103/PhysRevE.77.041112 PACS number(s): 05.50.+q, 64.60.−i, 75.10.Nr, 05.70.Fh

I. INTRODUCTION

The Blume-Emery-Griffiths (BEG) model [1] is a spin-1 Ising model with bilinear (J_{ij}), biquadratic (K_{ij}), and crystal-field interaction (Δ_{ij}) terms as shown in the Hamiltonian in Eq. (1)

$$-\beta H = \sum_{\langle ij \rangle} J_{ij} s_i s_j + \sum_{\langle ij \rangle} K_{ij} s_i^2 s_j^2 - \sum_{\langle ij \rangle} \Delta_{ij} (s_i^2 + s_j^2)$$

$$\text{with } s_i = 0, \pm 1, \tag{1}$$

The bilinear interactions directly affect magnetic ordering, whereas the other two terms primarily affect the relative density ($\sim \Delta/J$) and clustering ($\sim K/J$) of occupied sites. Systems with fluctuations in both density and magnetization are particularly well suited for investigation using this model. The Hamiltonian in Eq. (1) involves three summations over nearest-neighbor $\langle ij \rangle$ pairs of our lattice unit structure including the crystal-field interaction term. Typically, the crystal-field interaction (Δ_i) involves a summation over lattice sites; however, this study has changed the summation from sites to bonds for computational convenience; the net result being that Δ in Eq. (1) is the chemical potential per bond divided by 2. Each site can assume one of three states: (i) $s_i=0$, synonymous with the presence of a nonmagnetic impurity, and (ii) and (iii) a site may be occupied by a spin which is in one of two states ($s_i = \pm 1$). Two-state systems, with density as an added degree of freedom, have been used to effectively study a wide range of systems: structural glasses [2], binary fluids, the superfluid transition in ^{3}He-^{4}He mixtures, materials with mobile defects, binary alloys, and frustrated percolation [3] corresponding to a version of the frustrated Ising lattice gas [4,5].

The complexity of the resulting phase diagrams is very rich due to underlying competing interactions in various Blume-Emery-Griffiths models. Many different types of competing interaction have been the focus of previous studies using the Blume-Emery-Griffiths model in conjunction with mean-field methods [6–8] and/or renormalization-group techniques [9,10].

In particular, renormalization-group analysis reveals tricritical and critical end point topologies linking first- and second-order phase boundaries for the case with $K>0$. For negative biquadratic coupling ($K<0$), mean-field calculations revealed two novel phases: one a high-entropy ferrimagnetic phase and the other displaying antiquadrupolar order (see Ref. [6]).

The effects of attractive and repulsive biquadratic interactions on the global phase space was considered by Sellitto *et al.* [7] using the replica symmetric mean-field approximation with quenched disorder in the bilinear interactions. A spin-glass phase was found with both first- and second-order transitions from the paramagnetic phase, the order of the transition being largely dependent upon the crystal-field interaction. This study also found, for strong repulsive ($K<0$) biquadratic interactions, an antiquadrupolar phase and at lower temperatures an antiquadrupolar spin-glass phase.

Snowman [11] employed renormalization-group techniques and a hierarchical lattice in a system with competing biquadratic and crystal-field interactions while the bilinear interaction remained uniform. Chaotic rescaling of the biquadratic interaction (K) and crystal-field interaction (Δ) was revealed along a high-temperature phase boundary separating two paramagnetic phases, dense and dilute. In a separate study, Snowman [12] used the BEG model in conjunction with a similar renormalization-group method to consider the effects of annealed vacancies or nonmagnetic impurities on ordering in a system with competing ferromagnetic and antiferromagnetic interactions.

The current investigation complements these earlier works as it probes frustration that arises due to competing biquadratic ($\pm K$) interactions while maintaining uniform bilinear and crystal-field interactions. This competition directly affects the clustering and density of nonmagnetic impurities. Thus, any two-state system susceptible to density fluctuations could potentially be considered with this model. All calculations have been conducted using a hierarchical lattice in conjunction with renormalization-group methods, mirroring the approach of previous studies [10–13]. The nature of

*FAX: (401) 456-8396. Dsnowman@ric.edu

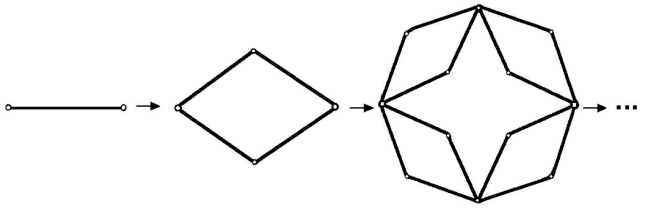

FIG. 1. In general, an infinite hierarchical lattice is generated from a basic unit by repeatedly replacing each nearest-neighbor interaction by the basic unit itself (Berker and Ostlund [14]).

each phase, and any associated transition(s), is ascertained from the renormalization-group trajectory. Phase diagrams have been generated probing the effects of these competing biquadratic interactions while varying the temperature and concentration of annealed vacancies.

II. HIERARCHICAL LATTICES AND RENORMALIZATION-GROUP THEORY

Figure 1 illustrates the construction of a general hierarchical lattice. Figure 2 illustrates the construction of the hierarchical lattice [14,15] used for this study. In general, an infinite hierarchical lattice is generated from its basic unit by repeatedly replacing each nearest-neighbor interaction by the basic unit itself. Hierarchical lattices are attractive to use as model systems since exact renormalization-group recursion relations can be calculated. Thus, phase diagrams can be produced and critical exponents determined with great precision. Therefore these results may be considered exact on the rather specialized lattice presented in this investigation, or they may be considered as approximations to the effects of competing biquadratic interactions on more realistic lattices. Hierarchical lattices have been used to successfully explore and understand a range of very complex problems. Included among these are spin-glass [16], frustrated [10], random-bond [17], random-field [18], directed-path [19], and dynamic scaling [20] systems.

The renormalization-group solution for a hierarchical model, such as Figs. 1 and 2, essentially reverses the construction process. Each renormalization eliminates internal degrees of freedom by summing over all configurations of the innermost sites [represented by solid black dots in Figs. 2(a) and 2(b) and by $\{\sigma_i,\sigma_j\}$ in Eq. (5)].

Preservation of the partition function at each length scale allows for the derivation of the recursion relations relating the interactions at the two length scales. The new effective interactions J', K', and Δ' are separated by a distance l', which is b lattice constants in the original system, where b is the length rescaling factor of the renormalization-group transformation:

$$\zeta_{l'}(J',K',\Delta') = \zeta_l(J,K,\Delta) \tag{2}$$

$$\text{with } l' = bl, \tag{3}$$

$$\zeta_l = \sum_{\{s\}} \exp(-\beta H) = \sum_{\{s_i,s_j\}} R_l(s_i,s_j) \tag{4}$$

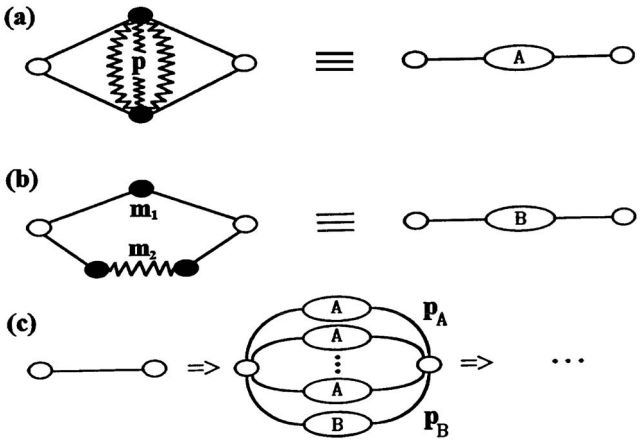

FIG. 2. Construction of the hierarchical lattice. Solid lines represent (J,K,Δ) nearest-neighbor site interactions, whereas jagged lines represent $(J,-K,\Delta)$ nearest-neighbor site interactions. In general, an infinite hierarchical lattice is generated from its basic unit by repeatedly replacing each nearest-neighbor interaction by the basic unit itself.

$$\text{with } R_l(s_i,s_j) = \sum_{\{\sigma_i,\sigma_j\}} \exp(-\beta H), \tag{5}$$

$$\zeta_{l'} = \sum_{\{s'\}} \exp(-\beta H') = \sum_{\{s_i',s_j'\}} R_{l'}(s_i',s_j') \tag{6}$$

$$\text{with } R_{l'}(s_i,s_j) = \exp[J' s_i s_j + K' s_i^2 s_j^2 - \Delta'(s_i^2 + s_j^2) + \tilde{G}], \tag{7}$$

where $\tilde{G}$ is a constant used to calculate the free energy.

The actual renormalization-group transformation is calculated by equating individual portions, $R_l(s_i,s_j)$ and $R_{l'}(s_i,s_j)$, of the summation for the partition function at each length scale. These contributions, $R_l(s_i,s_j)$ and $R_{l'}(s_i,s_j)$, correspond to the same fixed configuration of end spins $\{s_i,s_j\}$ at the two different length scales l and l'. From the resulting equations, the relations between interaction strengths at the two length scales l and l' can be derived: J' (J,K,Δ), K' (J,K,Δ), and Δ' (J,K,Δ). The reader is directed to Sec. IV for a derivation of these relations.

Phase diagrams are mapped and transitions characterized using these recursion relations in conjunction with the initial values of J, K, and Δ, and the resulting sink(s) of the renormalization-group trajectories:

$$J' = R_J(J,K,\Delta), \tag{8}$$

$$K' = R_K(J,K,\Delta), \tag{9}$$

$$\Delta' = R_\Delta(J,K,\Delta). \tag{10}$$

Each phase has associated with it a corresponding phase sink (see Table I), at which the values of the interactions (J,K,Δ) have reached a fixed point denoted by (J^*,K^*,Δ^*). In the vicinity of these fixed points the system is scale invariant and hence renormalization does not affect the properties of the system as the length scale is increased by a factor of b. The

TABLE I. The sinks, and associated phases, for the three unique basins of attraction.

Phase or basin	Sink	Characteristics
Ferromagnetic	$J\to+\infty$ $K\to-\infty$ $\Delta\to-\infty$	$\lvert K\rvert=\lvert J\rvert$ $\lvert\Delta\rvert\gg\lvert K\rvert,\lvert J\rvert$
Dense paramagnetic	$J\to 0$ $K\to 0$ $\Delta\to-\infty$	Disordered (magnetization=0)
Dilute paramagnetic	$J\to 0$ $K\to 0$ $\Delta\to+\infty$	Disordered (magnetization=0)

fixed points must satisfy the recursion relations such that

$$J^* = R_J(J^*,K^*,\Delta^*), \tag{11}$$

$$K^* = R_K(J^*,K^*,\Delta^*), \tag{12}$$

$$\Delta^* = R_\Delta(J^*,K^*,\Delta^*). \tag{13}$$

Two types of components [see Figs. 2(a) and 2(b)] have been included in the basic unit for the calculations presented in this paper, similar to the calculation of McKay *et al.* [10]. Each component contains two qualitatively different types of nearest-neighbor sites: those with interactions (J,K,Δ) and those with interactions $(J,-K,\Delta)$. When K is chosen so that simultaneous occupation is energetically favorable for nearest-neighbor sites with (J,K,Δ) interactions, it is unfavorable for nearest-neighbor sites with $(J,-K,\Delta)$ interactions, and vice versa.

These two qualitatively unique competing interactions allow us to separate the hierarchical lattice into two sublattices, distinguished from one another by the type of biquadratic interaction, attractive $(K>0)$ or repulsive $(K<0)$. Since some sites are connected to neighbors by each type of interaction, it is really the bonds, rather than the sites, that are associated with each sublattice and must be used in interpreting the phase associated with each sink.

Spatial frustration arises as a direct result of the positioning of the competing attractive $(K>0)$ and repulsive $(K<0)$ biquadratic interactions. The degree of the competition is tuned by varying the strength of the cross-link interaction [Fig. 2(a)]. The case of $p=0$ yields a hierarchical model that is equivalent [14] to the Migdal-Kadanoff [21,22] decimation-bond moving scheme in two dimensions. For this study, the cross-link interaction (p) in Fig. 2(a) has been chosen such that the spatial frustration present is at a maximum.

Figure 2(b) includes in the model the possibility of additional connecting paths between the end spins which may not have the cross-linked feature in Fig. 2(a). One type of path, consisting of m_1 pairs of spins, has all interactions of the same type, (J,K,Δ), while the other, with m_2 pairs of spins, has one nearest-neighbor pair that differs in the biquadratic interaction, $(J,-K,\Delta)$, from the rest of the connecting path.

The cross-linked structure [Fig. 2(a)] and the two different types of connecting paths [Fig. 2(b)] represent the two generically different types of geometries that could occur in real materials with density fluctuations and/or spatial inhomogeneities, such as a ferrofluid in a random medium. In systems such as these, sites separated by some distance are connected by multiple paths, some with and some without competing interactions.

The connectivity of the system is varied using two parameters p_A and p_B. These parameters, representing the number of unit structures, either type A or type B (see Fig. 2), are used to form the basic unit or generator for the hierarchical lattice as shown in Fig. 2(c). The competing mechanisms included in this study for the density degrees of freedom parallel those introduced for the orientational degrees of freedom in previous works [10,23]. In fact, this study has used the same connectivity values $(p,m_1,m_2,p_A,p_B)=(4,8,9,40,1)$, as Refs. [10,23]. Spin-glass systems reveal that a certain level of connectivity is necessary before the effects of competing interactions are observed; this observation is entirely consistent with other systems characterized by competing microscopic interactions (see Kauffman *et al.* [15]).

III. CHARACTERIZATION OF TRANSITIONS

Densities, magnetizations, and nearest-neighbor correlations can all be calculated by numerically differentiating the free energy with respect to the appropriate variables. The free energy density (dimensionless free energy per bond) f can be expressed as

$$f = \frac{-bF}{N_b} = \sum_{n=1}^{\infty} b^{-nd}\tilde{G}^{(n)}(J^{(n-1)},K^{(n-1)},\Delta^{(n-1)}), \tag{14}$$

where F is the Helmholtz free energy and N_b denotes the total number of bonds in the system. The free energy density consists of a sum over all iterations of the renormalization-group transformation of the contributions $\tilde{G}^{(n)}$ to the free energy density due to the degrees of freedom removed during each transformation. Each implementation of the renormalization-group transformation reduces the length scale of the system by a factor of b and the number of spins by a factor of b^d.

The free energy density allows us to calculate all thermodynamic quantities. The magnetization $m \equiv \frac{M}{N_s} = \frac{N_b}{N_s}\frac{\partial f}{\partial H}$, can be calculated by numerically measuring the shift in the free energy density with a small perturbation in the magnetic field, where N_s is the number of sites. In a like manner, the density can be calculated by differentiating the free energy density with respect to the crystal-field coefficient, $\rho \equiv \frac{N_b}{N_s}\frac{\partial f}{\partial \Delta}$. In addition to magnetization and density, correlations of the bilinear, $\langle s_i s_j\rangle = N_b\frac{\partial f}{\partial J_{ij}}$, and biquadratic, $\langle s_i^2 s_j^2\rangle = N_b\frac{\partial f}{\partial K_{ij}}$, exchange interactions are also valuable when interpreting the phases and characterizing transitions. Since our unit structure consists of two different types of nearest-neighbor interactions, the above thermodynamic quantities were calculated separately for each type of nearest-neighbor pair $(J,-K,\Delta)$ and

(J,K,Δ). This approach leads to easier interpretations of the spin configurations associated with each phase.

Equipped with values for the four thermodynamic quantities discussed above, transitions between the various basins of attraction are characterized for each sublattice. Recall that first-order transitions are characterized by discontinuities in densities, magnetizations, or other first derivatives of the free energy, whereas second-order or continuous transitions exhibit no such discontinuities. It is important to note that exact knowledge of the recursion relations allows us to calculate critical scaling exponents as second-order transitions are encountered in our phase space. The next section explores this in greater detail.

IV. RECURSION RELATIONS

By equating the contributions to the partition function from the two length scales, for each fixed end spin configuration, we can write the following equalities for the type A structure shown in Fig. 2(a).

$$\begin{aligned} R_l(1,1) &= \exp[(p+4)J + (4-p)K - (2p+8)\Delta] \\ &\quad + 2\exp[2J + 2K - (p+6)\Delta] \\ &\quad + 2\exp[-pJ + (4-p)K - (2p+8)\Delta] + \exp(-4\Delta) \\ &\quad + 2\exp[-2J + 2K - (p+6)\Delta] \\ &\quad + \exp[(p-4)J + (4-p)K - (2p+8)\Delta] \\ &= \exp(J' + K' - 2\Delta' + \tilde{G}) = R_{l'}(1,1), \end{aligned} \tag{15}$$

$$\begin{aligned} R_l(1,0) &= \exp[(2+p)J + (2-p)K - (2p+6)\Delta] \\ &\quad + 2\exp[J + K - (p+4)\Delta] \\ &\quad + 2\exp[-pJ + (2-p)K - (2p+6)\Delta] + \exp(-2\Delta) \\ &\quad + 2\exp[-J + K + (p+4)\Delta] \\ &\quad + \exp[(2-p)J + (2-p)K - (2p+6)\Delta] \\ &= \exp(-\Delta' + \tilde{G}) = R_{l'}(1,0), \end{aligned} \tag{16}$$

$$\begin{aligned} R_l(1,-1) &= 2\exp[pJ + (4-p)K - (2p+8)\Delta] \\ &\quad + 2\exp[-pJ + (4-p)K - (2p+8)\Delta] \\ &\quad + \exp(-4\Delta) + 4\exp[2K - (p+6)\Delta] \\ &= \exp(-J' + K' - 2\Delta' + \tilde{G}) = R_{l'}(1,-1), \end{aligned} \tag{17}$$

$$\begin{aligned} R_l(0,0) &= 2\exp[pJ - pK - (2p+4)\Delta] + 4\exp[-(p+2)\Delta] \\ &\quad + 2\exp[-pJ - pK - (2p+4)\Delta] + 1 \\ &= \exp(\tilde{G}) = R_{l'}(0,0). \end{aligned} \tag{18}$$

Using the relationships above [Eqs. (15)–(18)], we can derive expressions relating the coupling coefficients between the two length scales for the type A unit structure:

$$J'_A = \frac{1}{2}\ln\left(\frac{R_{l'}(1,1)}{R_{l'}(1,-1)}\right), \tag{19}$$

$$K'_A = \frac{1}{2}\ln\left(\frac{R_{l'}(1,1)R_{l'}(1,-1)R^2_{l'}(0,0)}{R^4_{l'}(1,0)}\right), \tag{20}$$

$$\Delta'_A = \ln\left(\frac{R_{l'}(0,0)}{R_{l'}(1,0)}\right), \tag{21}$$

$$\tilde{G}'_A = \ln R_{l'}(0,0). \tag{22}$$

The recursion relations for simpler (type B) unit structures have the same form as in Eqs. (19)–(22), but the expressions [Eqs. (15)–(18)] for the corresponding $R_l(s_i,s_j)$ differ. Combining the recursion relationships for both types of structure (A and B as shown in Fig. 2), the renormalization relationships become

$$J' = p_A J'_A + p_B J'_B, \tag{23}$$

$$K' = p_A K'_A + p_B K'_B, \tag{24}$$

$$\Delta' = p_A \Delta'_A + p_B \Delta'_B. \tag{25}$$

The exact recursion relations above can be used to calculate critical exponents by linearizing the recursion relations in the vicinity of the second-order transition under investigation. That is,

$$J' - J^* = T_{JJ}(J - J^*) + T_{JK}(K - K^*) + T_{J\Delta}(\Delta - \Delta^*), \tag{26}$$

$$K' - K^* = T_{KJ}(J - J^*) + T_{KK}(K - K^*) + T_{K\Delta}(\Delta - \Delta^*), \tag{27}$$

$$\Delta' - \Delta^* = T_{\Delta J}(J - J^*) + T_{\Delta K}(K - K^*) + T_{\Delta\Delta}(\Delta - \Delta^*), \tag{28}$$

where $T_{JJ}=\frac{\partial J'}{\partial J}$, $T_{KJ}=\frac{\partial K'}{\partial J}$, etc. and they are evaluated at the fixed point in question. The critical relations above can be represented as a recursion matrix, with elements T_{XY} and eigenvalues of the form

$$\Lambda_l = b^{y_l}, \tag{29}$$

where b is the length rescaling factor (in our case $b=2$) and y_l represents the corresponding critical exponent for the lth eigenvalue.

V. RESULTS

Below we consider a series of planes of constant K/J while the temperature ($\sim 1/J$) and vacancy concentration ($\sim \Delta/J$) present in the system are varied. In each plane, we have mapped out the different regions of parameter space according to the renormalization-group trajectories that arise. This investigation reveals three qualitatively unique regions (or basins of attraction), each sharing renormalization-group trajectories that flow to common sinks or attractors (see Table I).

Two basins arise in parameter space in which bilinear (J) and biquadratic (K) renormalization-group trajectories flow

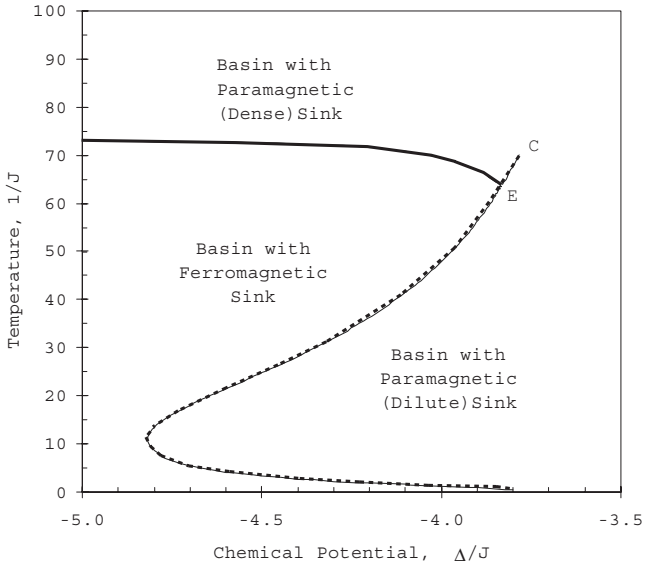

FIG. 3. Parameter space, with $K/J=-5$ and $(p,m_1,m_2,p_A,p_B)=(4,8,9,40,1)$, depicting different basins of attraction and associated phases with critical end point (E) and critical point (C). Solid lines represent second-order transitions, whereas dashed lines represent first-order transitions.

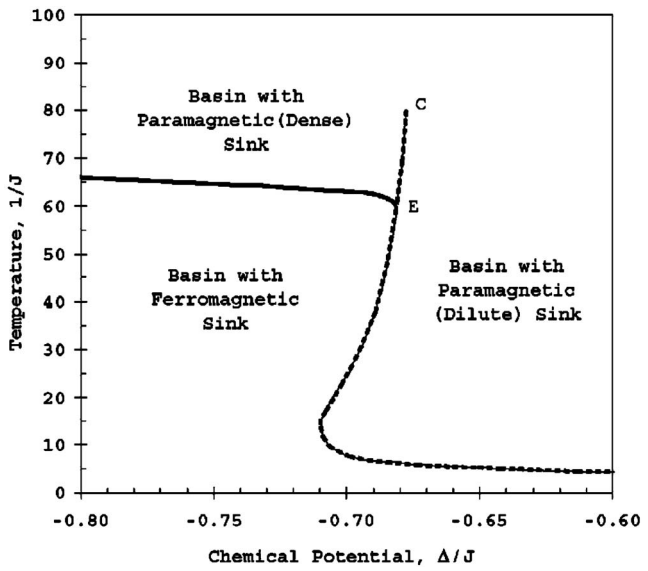

FIG. 4. Parameter space, with $K/J=-1$ and $(p,m_1,m_2,p_A,p_B)=(4,8,9,40,1)$, depicting different basins of attraction and associated phases with critical end point (E) and critical point (C). Solid lines represent second-order transitions, whereas dashed lines represent first-order transitions.

to zero, indicating that long-range order does not propagate. The sinks for both of these basins correspond to paramagnetic states. These paramagnetic states are distinguished from one another only by the renormalization-group trajectory of the crystal-field interaction (Δ/J), thus affecting the concentration of vacancies in each case. Although the vacancy concentration is low in the dense paramagnetic state, the temperature is too high for the system to order (see Figs. 3–6). The dilute paramagnetic state is present at all temperatures (see Figs. 3–6) but cannot order since the vacancy concentration is too high for long-range order to develop.

The third basin (dense ferromagnetic) that arises in parameter space has a sink with renormalization-group trajectories that indicate magnetic ($J\rightarrow+\infty$) and spatial ($K\rightarrow-\infty$) ordering, as well as low vacancy concentration ($\Delta\rightarrow-\infty$).

In the plane of $K/J=-5$ (Fig. 3) we find regions with renormalization-group trajectories flowing to each of the sinks detailed above. The ordered ferromagnetic phase disorders as temperature is increased to a dense paramagnetic state via a second-order phase transition. This critical line terminates at a critical end point (E) on a line of first-order transitions, similar to that topology observed by Hoston and Berker [6], for the case of uniform J, K, and Δ with $K/J=5$, using mean-field theory. This line of first-order transitions separates the ordered ferromagnetic phase from the dilute paramagnetic state at low temperatures, and at higher temperatures it separates the dense and dilute paramagnetic states before terminating at critical point C at $1/J\cong 70$. Also of particular note in this phase diagram is the doubly reentrant topology between the different basins of attraction (ferromagnetic–dilute paramagnetic–ferromagnetic–dense paramagnetic) in the range $-4.8<\Delta/J<-3.9$. This double reentrance disappears as the spin-1/2 Ising limit ($\Delta/J->-\infty$) is approached.

Similar calculations for the $K/J=-1$ plane show that the qualitative nature of the phase diagram remains the same, complete with the critical end point (E) and critical point (C) topology seen for $K/J=-5$. However, the prominence of the doubly reentrant region of the phase diagram is diminished and occurs over a much smaller range of Δ/J, as shown in Fig. 4. The first-order phase boundary separating the two paramagnetic regions terminating at the critical point (C) is shifted to higher temperatures ($1/J\cong 80$) as K/J is increased.

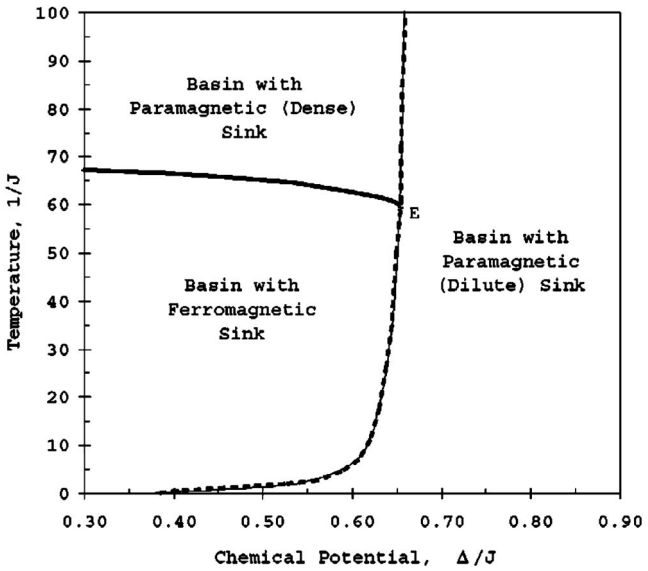

FIG. 5. Parameter space, with $K/J=1$ and $(p,m_1,m_2,p_A,p_B)=(4,8,9,40,1)$, depicting different basins of attraction and associated phases with critical end point (E). Solid lines represent second-order transitions, whereas dashed lines represent first-order transitions.

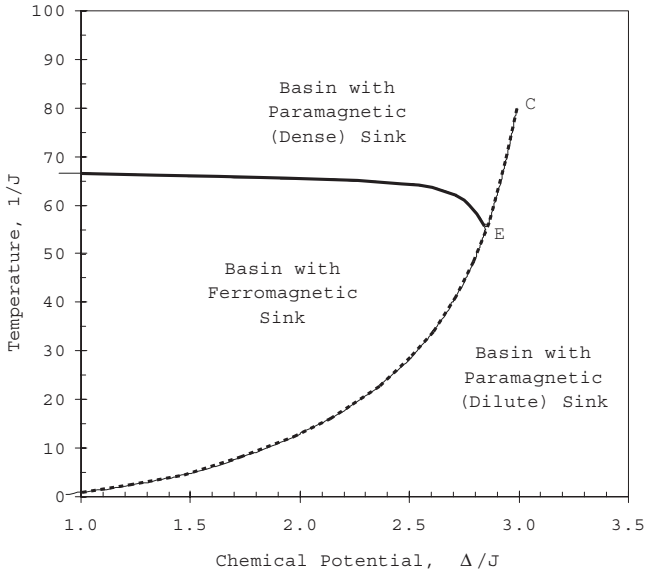

FIG. 6. Parameter space, with $K/J=5$ and $(p,m_1,m_2,p_A,p_B)=(4,8,9,40,1)$, depicting different basins of attraction and associated phases with critical end point (E) and critical point (C). Solid lines represent second-order transitions, whereas dashed lines represent first-order transitions.

One can go smoothly between the dense and dilute paramagnetic phases at temperatures above the critical point, as in the standard liquid-gas phase diagram.

Positive clustering bias ($K/J=1$) results in a phase diagram (Fig. 5) in which the boundary between the dense ferromagnetic and dilute paramagnetic basins has shifted to larger Δ/J, while the topology of the boundary separating the dense paramagnetic and ferromagnetic basins remains qualitatively the same and occurs at approximately the same temperature. The critical point (C) terminating the line of first order transitions between dense and dilute paramagnetic phases has shifted to $1/J\cong 180$ (not shown in the figure). Reentrance to a disordered (paramagnetic) region occurs over a wide range of Δ/J (annealed vacancy concentrations). As the temperature is lowered at fixed chemical potential a paramagnetic (dense)–ferromagnetic–paramagnetic (dilute) sequence of transitions is encountered.

As the clustering bias is further increased to $K/J=5$ (Fig. 6), the critical end point (E) and critical point (C) topology remains, yet the boundary separating the ferromagnetic and dilute paramagnetic basins has curved so drastically that it is possible to order the dilute paramagnetic phase at high temperatures by further *increasing* the temperature over a broad range of Δ/J. The critical point (C) terminating the line of first-order transitions has shifted to $1/J\cong 80$. It is also apparent that a changing temperature can drive the system from one paramagnetic basin to the other (Fig. 6). The boundary separating the dense paramagnetic and ferromagnetic basins remains qualitatively the same and is located at approximately the same temperature.

In each of the four planes of constant biquadratic coupling, the high-temperature transition from the dense ferromagnetic phase to the dense paramagnetic phase was found to be second order. In this study, we have probed this critical line while maintaining three scaling fields associated with J, K, and Δ. Linearizing the recursion relations, as discussed in Sec. IV, yields a recursion matrix with two relevant eigenvalues $\Lambda_1=2$ and $\Lambda_2=2$, corresponding to critical scaling exponents of $y_1=1$ and $y_2=1$, respectively. The third eigenvalue is irrelevant with $\Lambda_3=0$. Work is currently ongoing that will introduce an additional scaling field associated with small perturbations of an external magnetic field (H).

VI. SUMMARY

In summary, this study considers an exactly solvable spin-1 Ising system in which frustration is present due to competing biquadratic interactions. Thus, this calculation models a dilute ferromagnetic material with two types of nearest-neighbor site pairs, distinguished by whether or not simultaneous occupation is energetically favored. The effects of these competing biquadratic interactions are probed by calculation of phase diagrams for a series of planes of constant biquadratic coupling while the temperature and concentration of annealed vacancies in the system are varied. Each phase diagram reveals three qualitatively unique basins of attraction, each sharing renormalization-group trajectories that flow to common sinks. Each sink corresponds to a different phase (ferromagnetic, dense paramagnetic, dilute paramagnetic) of the system.

Planes of negative K/J result in phase diagrams that exhibit double reentrance with the phase sequence ferromagnetic–paramagnetic (dilute)–ferromagnetic–paramagnetic (dense) encountered with increasing temperature. Planes of constant clustering bias corresponding to attractive ($K>0$) biquadratic couplings show reentrance, with the phase sequence paramagnetic (dilute)–ferromagnetic–paramagnetic (dense) encountered as temperature is increased at fixed chemical potential. In each plane of constant biquadratic coupling, the critical line separating the ferromagnetic and dense paramagnetic states terminates at a critical end point (E) on a line of first-order transitions, itself terminating at a critical point (C) at higher temperatures. Most intriguing is the ordering of the dilute paramagnetic phase at high temperatures by further *increasing* the temperature. These results may offer insights into other systems characterized by density fluctuations and spatial inhomogeneities as a result of competing interactions.

ACKNOWLEDGMENTS

The author of this paper is indebted to Professor Susan R. McKay of the University of Maine for her guidance, support, and suggestion of this problem. Also, the author extends thanks to Rhode Island College for granting release time in support of this work.

[1] M. Blume, V. J. Emery, and R. B. Griffiths, Phys. Rev. A **4**, 1071 (1971).
[2] T. R. Kirkpatrick and D. Thirumalai, Phys. Rev. B **36**, 5388 (1987).
[3] A. Coniglio, J. Phys. IV **3**, C1-1 (1993); Nuovo Cimento D **16**, 1027 (1994).
[4] J. J. Arenzon, M. Nicodemi, and M. Sellitto, J. Phys. I **6**, 1143 (1996).
[5] M. Nicodemi and A. Coniglio, J. Phys. A **30**, L187 (1997).
[6] W. Hoston and A. N. Berker, Phys. Rev. Lett. **67**, 1027 (1991).
[7] M. Sellitto, M. Nicodemi, and J. J. Arenzon, J. Phys. I **7**, 945 (1997).
[8] S. R. McKay and A. N. Berker, J. Appl. Phys. **55**, 1646 (1984).
[9] A. N. Berker and M. Wortis, Phys. Rev. B **14**, 4946 (1976).
[10] S. R. McKay, A. N. Berker, and S. Kirkpatrick, Phys. Rev. Lett. **48**, 767 (1982).
[11] D. P. Snowman, J. Magn. Magn. Mater. **314**, 69 (2007).
[12] D. P. Snowman, J. Magn. Magn. Mater. **320**, 1622 (2008).
[13] D.P. Snowman, Ph.D. thesis, University of Maine, 1995.
[14] A. N. Berker and S. Ostlund, J. Phys. C **12**, 4961 (1979).
[15] M. Kaufman and R. B. Griffiths, Phys. Rev. B **24**, 496 (1981).
[16] G. Migliorini and A. N. Berker, Phys. Rev. B **57**, 426 (1998).
[17] D. Andelman and A. N. Berker, Phys. Rev. B **29**, 2630 (1984).
[18] A. Falicov, A. N. Berker, and S. R. McKay, Phys. Rev. B **51**, 8266 (1995).
[19] R. A. da Silveira and J. P. Bouchaud, Phys. Rev. Lett. **93**, 015901 (2004).
[20] R. B. Stinchcombe and A. C. Maggs, J. Phys. A **19**, 1949 (1986).
[21] A. A. Migdal, Zh. Eksp. Teor. Fiz. **69**, 1457 (1975) [Sov. Phys. JETP **42**, 743 (1976)].
[22] L.P. Kadanoff, Ann. Phys. (N.Y.) **100**, 359 (1976).
[23] S. R. McKay, A. N. Berker, and S. Kirkpatrick, J. Appl. Phys. **53**, 7974 (1982).